JOURNAL OF MATERIALS SCIENCE 23 (1988) 2205–2212

Electrical conduction in thin films of CeO_2/GeO_2

Z. T. AL-DHHAN, C. A. HOGARTH
Department of Physics, Brunel University, Uxbridge, Middlesex, UK

A.c. and d.c. conduction in MIM sandwich structures based on CeO_2/GeO_2 as a dielectric prepared by the co-evaporation technique has been investigated for samples having different compositions. A transition of electrical conductivity from amorphous semiconductor to metallic behaviour as the temperature increased is reported. The electroformed samples show a voltage-controlled negative resistance (VCNR) at high values of bias voltage.

1. Introduction

The electrical properties of thin oxide films are of current interest, partly because some behave as good dielectric materials while others make transparent conducting electrodes. Recently, Al-Dhhan and Hogarth [1] have reported the properties of thin CeO_2 films which show a number of interesting properties when regarded as MIM devices. Khan *et al.* [2, 3] reported properties of thin GeO_2 films which show electroforming, voltage-controlled differential negative resistance, electron emission, switching and memory effects, while Hogarth and Rahman [4] described the mixed system of SiO/GeO_2 made by the co-evaporation technique. Al-Ramadhan *et al.* [5] reported the time dependence associated with the memory states for the SiO/GeO_2 mixed system.

2. Experimental work

The CeO_2/GeO_2 films were prepared by the co-evaporation technique described by Hogarth and Wright [6] in a vacuum of 8×10^{-6} torr in a Balzers BA 510 coating unit. A tungsten boat was used for CeO_2 while GeO_2 was evaporated from a molybdenum boat, and the Corning 7059 glass substrates were kept at a temperature of 100° C. Each substrate supported several samples each of active area $0.15\,cm^2$. Electrical measuring techniques were described in an earlier work [1].

3. D.c. conduction before electroforming

Typical V_b–I_c characteristics of CeO_2/GeO_2 MIM structures having different compositions are shown in Fig. 1, V_b being the applied voltage and I_c the circulating current. Up to 1 V applied the conduction is ohmic and various parameters were derived in this region as shown in Table I, where the values are typical of amorphous semiconductor materials.

The analyses of these curves are shown in Fig. 2, where log I_c is plotted as function of $V_b^{1/2}$ and the relation is indicative of either Schottky emission [7] or Poole–Frenkel emission [8]. Both phenomena are described by

$$I_c \propto \exp \frac{\beta E^{1/2}}{kT} \quad (1)$$

where E is the applied field ($= V_b/d$) d being the insulator thickness, k is the Boltzmann constant, T is the absolute temperature and β is the field lowering coefficient given by

$$\beta = \left(\frac{e^3}{n\pi\varepsilon_0\varepsilon_r}\right)^{1/2} \quad (2)$$

where ε_0 is the permittivity of free space, ε_r is the relative permittivity of the dielectric, and n is a constant ($n = 1$ for Poole–Frenkel and $n = 4$ for Schottky emission). The experimental values for the lowering coefficient, β, and relative permittivity of the dielectric, ε_r, for a film thickness of 300 nm are given in Table II. The results are in favour of the Poole–Frenkel mechanism which gives more reliable values for the dielectric constant. Figs 3a, b and c show log I_c plotted against log V_b for 300 nm thick $Al–CeO_2/GeO_2–Al$ samples at different temperatures. The dependence is typical of what have been observed with most amorphous semiconductors and insulators. These curves may be explained in terms of the Poole–Frenkel effect, with a log I_c–$V_b^{1/2}$ dependence as shown in Figs 4a, b and c. The values of the dielectric constant, ε_r, and the field lowering coefficient, β, are shown in Table III. Above room temperature a decrease in the dielectric constant, ε_r, accompanied by

TABLE I

Composition (mol %)		Circulating current, I_c (A)	Conductance, G (Ω^{-1})	Conductivity, σ ($\Omega^{-1}\,cm^{-1}$)	Resistivity, ϱ (Ω cm)
CeO_2	GeO_2				
94	6	1.70×10^{-7}	1.7×10^{-7}	3.4×10^{-11}	2.9×10^{10}
75	25	6.20×10^{-7}	6.2×10^{-7}	1.2×10^{-10}	8.1×10^{9}
60	40	1.85×10^{-6}	1.9×10^{-6}	3.7×10^{-10}	2.7×10^{9}
40	60	1.40×10^{-5}	1.4×10^{-5}	2.8×10^{-9}	3.6×10^{8}

0022–2461/88 \$03.00 + .12 © 1988 Chapman and Hall Ltd.

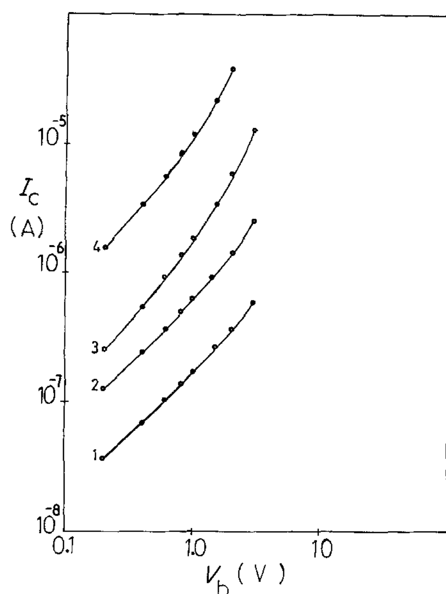

Figure 1 Voltage–current characteristics of 300 nm thick films of Al–CeO_2/GeO_2–Al: (1) 94 mol % CeO_2, (2) 75 mol % CeO_2, (3) 60 mol % CeO_2, (4) 40 mol % CeO_2.

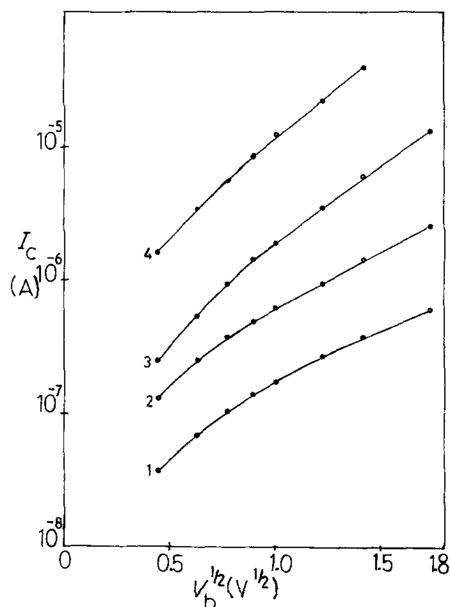

Figure 2 I_c–$V_b^{1/2}$ characteristics for different compositions of CeO_2/GeO_2 thin films: (1) 94/6, (2) 75/25, (3) 60/40, (4) 40/60.

an increase in the lowering coefficient, β, is observed and below room temperature the values of ε_r are found to be increased and accompanied by a decrease in β.

4. Transition from hopping conductivity to free band conductivity

Some electrons will gain sufficient energy to move into the states in the conduction band when the temperature increased. As the free band mobility is much greater than the hopping mobility, this process is accompanied by a sharp rise in the conductivity. This transition from localized state to free band conduction is illustrated in Fig. 5a for 25 mol % CeO_2/75 mol % GeO_2 and in Fig. 5b for 40 mol % CeO_2/60 mol % GeO_2. At low temperature the hopping conduction is dominant with an activation energy $\Delta E \approx 0.07$ and 0.015 eV, respectively, the same values being obtained at different applied voltages. A gradual transition occurs to a free band conduction as the temperature is raised and this may be due to some overlapping of the localized level and conduction band, as would be the case if the Fermi level fell in the vicinity of the transition from free band to the localized tail. The associated free band activation energy is 0.54 eV for 25 mol % CeO_2/75 mol % GeO_2 and 0.32 eV for 40 mol % CeO_2/60 mol % GeO_2.

It is noted that when the germanium oxide concentration is greater than 25 mol % and less than 75 mol %, a decrease of the slope d ln I_c/d$(1/T)$ is observed at high temperature, i.e. a levelling off of the current as shown in Figs 6a, b and c. This suggests a gradual transition from amorphous to metallic type of behaviour as the temperature is raised.

A film of 45 mol % CeO_2/55 mol % GeO_2, 10 nm thick, deposited on to carbon-coated mica, was used for study by transmission electron microscopy. A typical micrograph with the surface seen to be smooth is shown in Fig. 7a but when the sample was heated up to 120° C, the surface appearance is changed as shown in Fig. 7b where metallic particles appear.

As the temperature increases, the conductivity would be changed as the Fermi level sweeps past the mobility edge. There will be sharp change in the conductivity only if the free band mobility is much greater than the hopping mobility as indicated previously. The general form of this process is expressed by the formula

$$\sigma = \sigma_0 \, e^{-\Delta E/kT} \tag{3}$$

where ΔE is the activation energy. The expression for the mobility, μ, in localized states is given by Mott [9]

$$\mu = \mu' \, e^{-\Delta E/kT} \tag{4}$$

which indicates that μ increases as T increases. For conduction in the extended states the corresponding theoretical expression (Rose *et al.* [10]) is of the form

$$\mu = \text{const.}\ T^{-3/2} \tag{5}$$

which leads to μ decreasing as T increases.

Transmission electron microscopy and the d.c. results (Fig. 6) show that the properties of the samples

TABLE II

Composition (mol %)		β_{exp} (10^{-4} eV cm$^{1/2}$ V$^{-1/2}$)	Relative permittivity, ε_r (estimated)	
CeO_2	GeO_2		(n = 4, Schottky)	(n = 1, Poole–Frenkel)
94	6	2.0	3.6	14.4
75	25	2.7	2.0	8.0
60	40	3.7	1.0	4.2
40	60	6.1	0.4	1.6

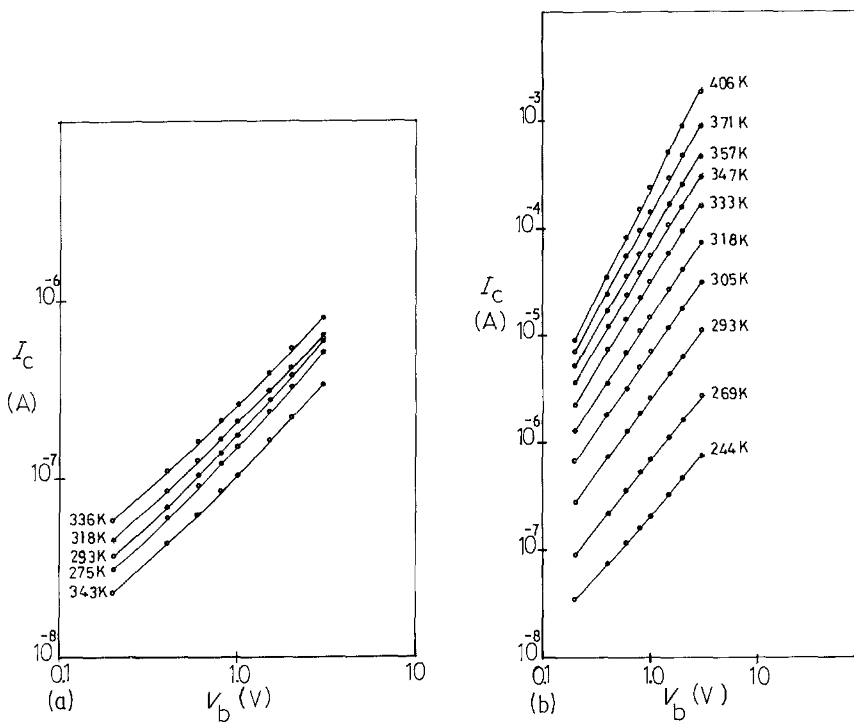

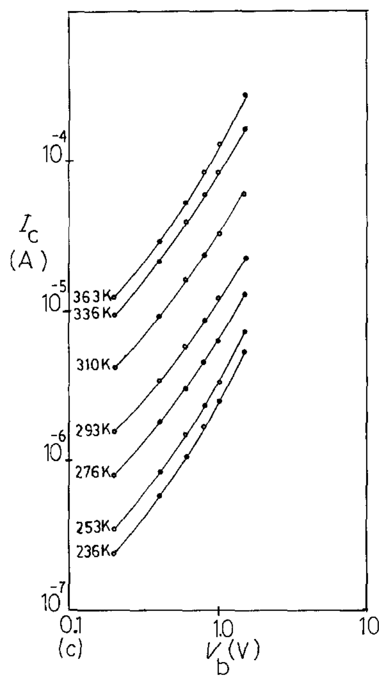

Figure 3 Voltage–current characteristics of 300 nm thick thin films at different temperatures: (a) 94 mol % CeO_2/6 mol % GeO_2, (b) 55 mol % CeO_2/45 mol % GeO_2, (c) 30 mol % CeO_2/70 mol % GeO_2.

change from amorphous to metallic behaviour and the conductivity will decrease as the temperature is increased because the charge carrier concentration remains constant and the mobility decreases with increasing temperature.

5. D.c. conduction after electroforming

Fig. 8 curve (a) shows the V_b–T_c characteristics of a 300 nm thick Cu–60 mol % CeO_2/40 mol % GeO_2–Cu sample which has been electroformed by applying a minimum forming voltage across it for a definite period of time. The result can be explained on a filamentary model of electrical conduction [11]. Conducting filaments made of chains of metal atoms alternating with anion vacancies develop across the insulating layer and bridge the electrode [12]. Conduction after

TABLE III

Composition of CeO_2/GeO_2 (mol %)	Temperature (K)	β_{exp} (10^{-4} eV cm$^{1/2}$ V$^{-1/2}$)	Relative permittivity, $(\varepsilon_r)_{PF}$
94/6	243	1.6	22.0
	293	2.0	14.4
	318	2.0	14.3
	336	2.1	13.6
55/45	244	2.1	13.5
	293	2.8	7.6
	347	3.6	4.6
	406	5.1	2.3
30/70	236	4.7	2.6
	293	4.9	2.4
	336	6.0	1.6
	363	7.3	1.1

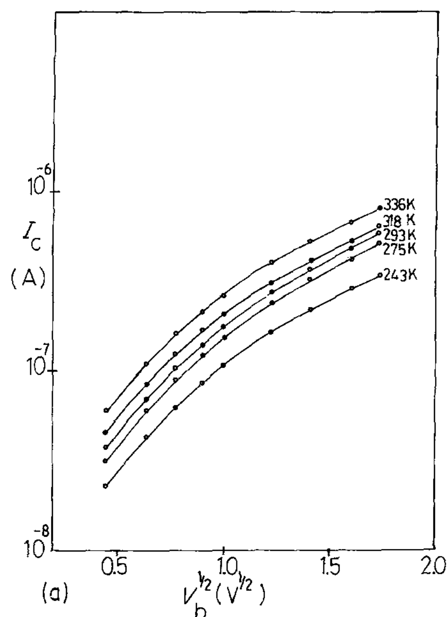

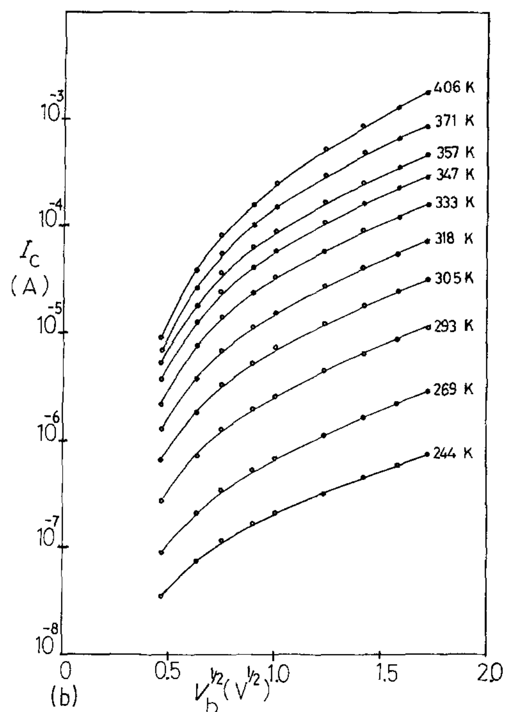

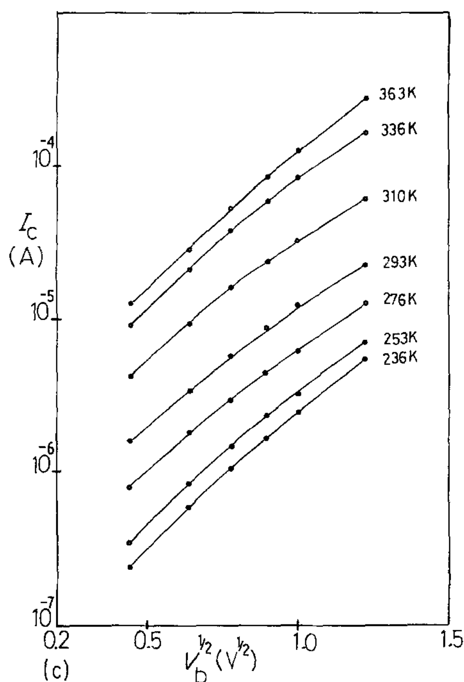

Figure 4 I_c–$V_b^{1/2}$ characteristics at different temperature for the samples in Fig.3.

electroforming takes place with the assistance of these filaments and hence the conductivity level increases. Because of large power dissipation at the maximum current, I_m, some of the filaments start rupturing at weak points resulting in a decrease of I_c and in the manifestation of VCNR. The filaments can regrow by some kind of ionic migration resulting in reproducible V_b–I_c characteristics. Fig. 8 curve (b) shows voltage memory exhibited by the sample at room temperature. It was found that a high resistance memory state could be induced if the voltage were lowered rapidly from any point on the VCNR trace to zero, followed by switching off the power supply for a very short time. When the voltage was re-applied the original high-resistance state was regenerated up to a particular

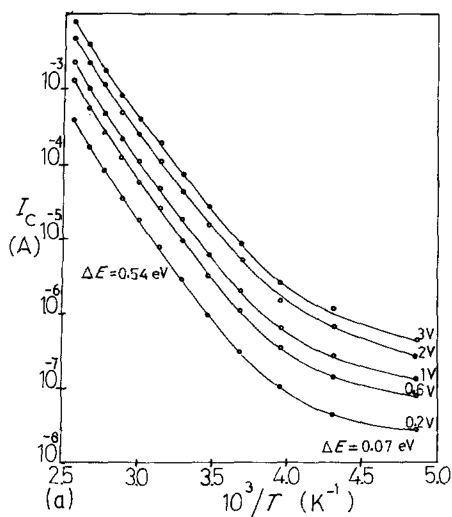

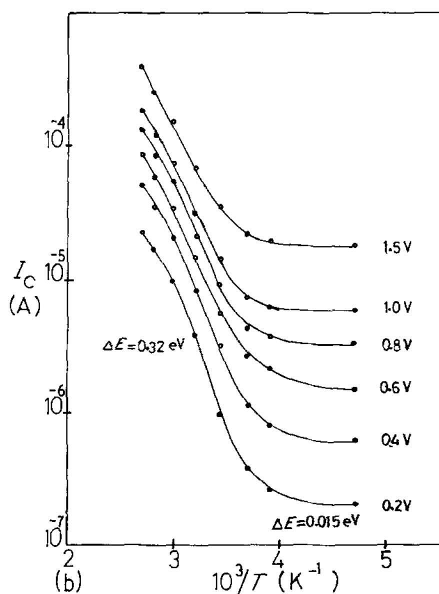

Figure 5 Temperature dependence of I_c as a function of inverse temperature for samples of thickness 300 nm (bias voltages shown). (a) 25 mol % CeO_2/75 mol % GeO_2, (b) 40 mol % CeO_2/60 mol % GeO_2.

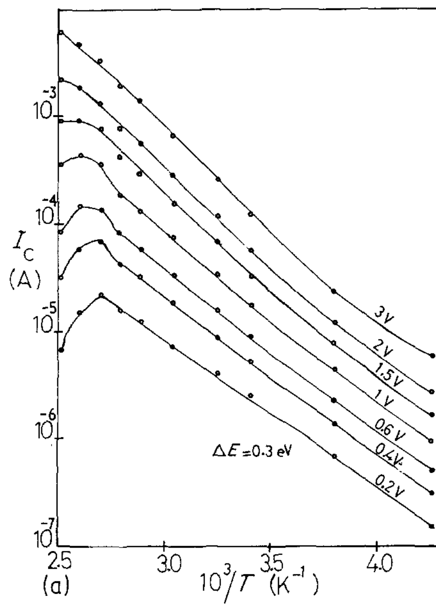

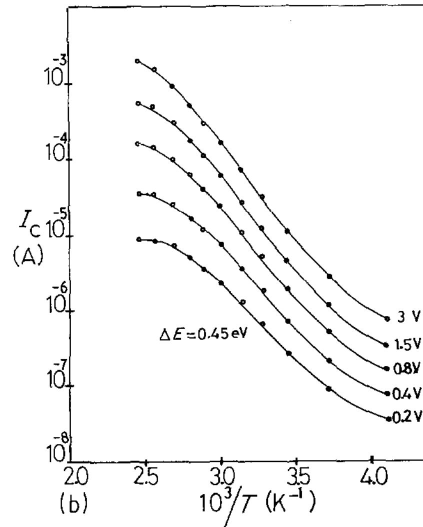

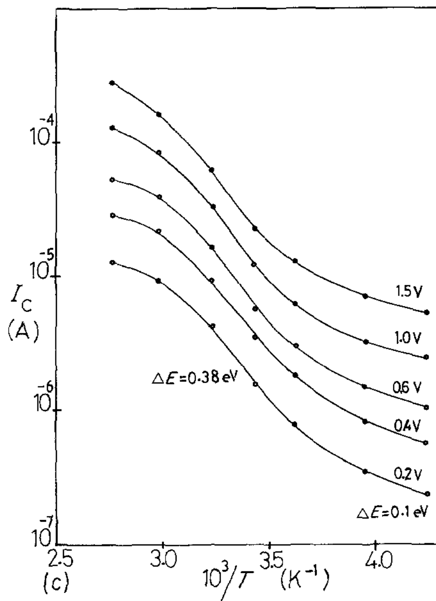

Figure 6 I_c–$1/T$ plots for films of thickness 300 nm for different bias voltages. (a) 60 mol % CeO_2/40 mol % GeO_2, (b) 55 mol % CeO_2/45 mol % GeO_2, (c) 30 mol % CeO_2/70 mol % GeO_2.

threshold voltage, where the current increased sharply to join up the previous high-conductivity state in the VCNR region. Voltage memory effects have been explained by Simmons and Verderber [13] and by Ralph and Woodcock [14].

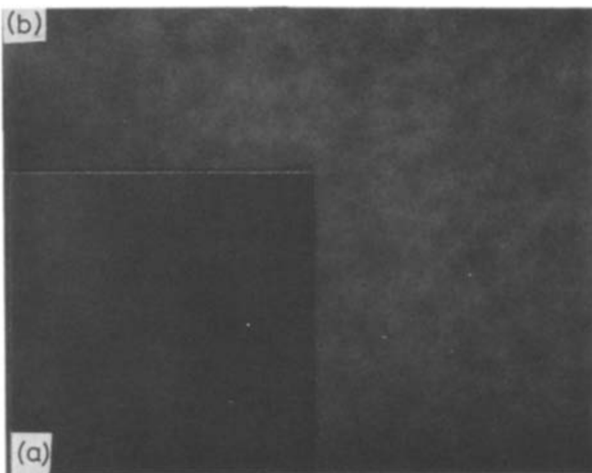

Figure 7 Transmission electron micrograph of samples, (a) at room temperature, (b) at 120° C.

6. A.c. conduction

A.c. conduction measurements were taken in the frequency range 10^2 to 10^6 Hz and different ranges of temperature for thin films of Al–CeO_2/GeO_2–Al as shown in Figs 9a, b and c for different compositions. The a.c. conductivity variation with frequency can be approximated as

$$\sigma_{a.c.} = \sigma_{tot} - \sigma_{d.c.} \qquad (6)$$

where $\sigma_{a.c.}$ is the a.c. electrical conductivity, σ_{tot} is the total conductivity and $\sigma_{d.c.}$ is the d.c. conductivity. Figs 10a, b and c show conductivity $\sigma(\omega)$ plotted against $1/T$ for the above samples. The results can be explained as follows. The electrical conductivity in an

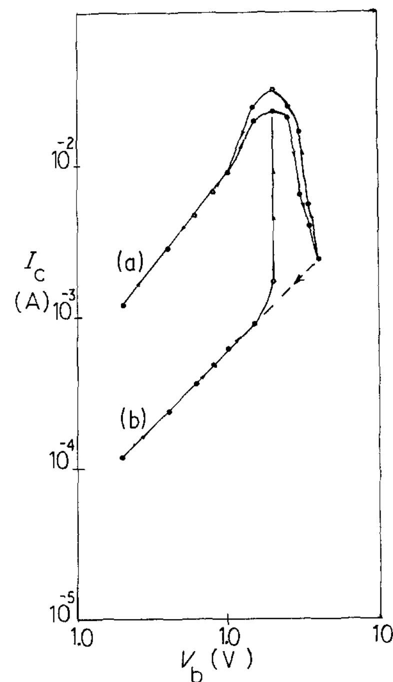

Figure 8 Voltage–current characteristics of Cu–40 mol % CeO_2/60 mol % GeO_2–Cu sample, (a) after forming, (b) voltage memory.

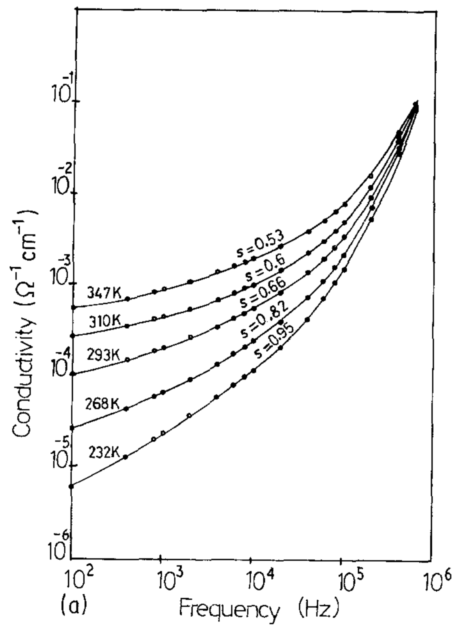

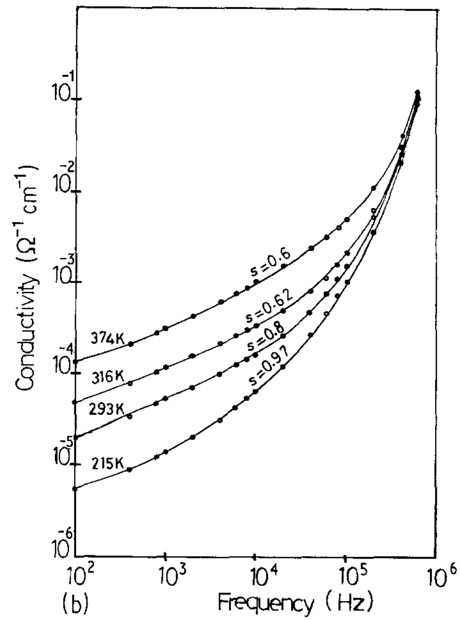

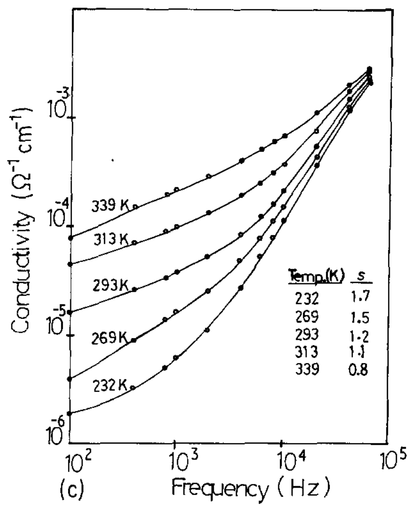

Figure 9 Variation of a.c. conductivity with frequency at different temperature for 300 nm thick thin films. (a) 60 mol % CeO_2/40 mol % GeO_2, (b) 40 mol % CeO_2/60 mol % GeO_2, (c) 30 mol % CeO_2/70 mol % GeO_2.

Figure 10 Conductivity plotted as a function of $1000/T$ for various fixed frequencies for the samples in Fig.9.

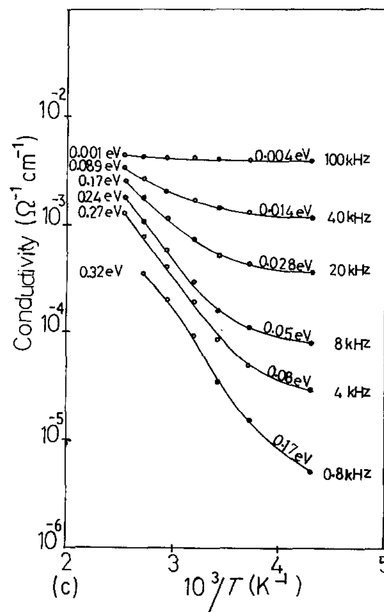

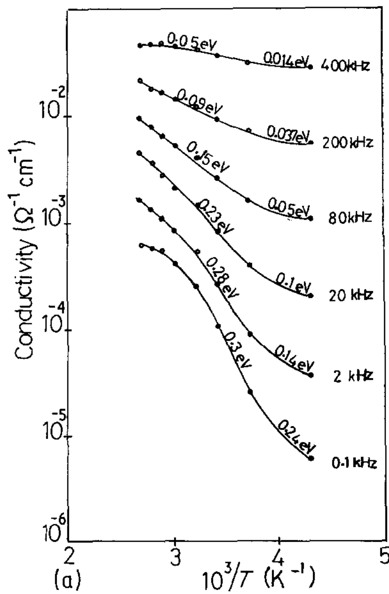

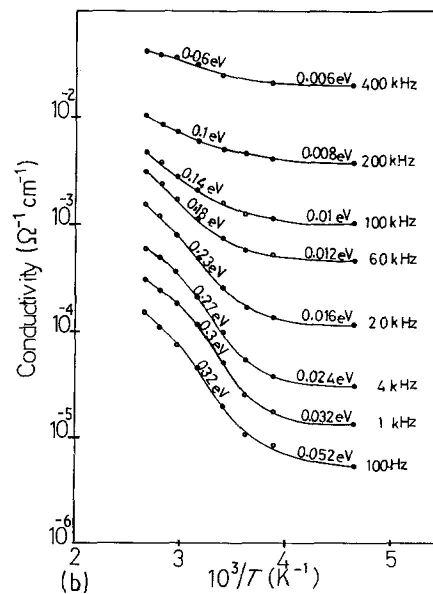

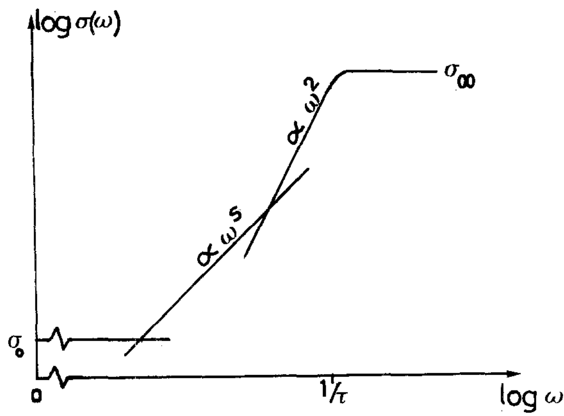

Figure 11 Schematic diagram of the frequency dependence of hopping conductivity; σ_0 is the d.c. conductivity.

alternating field may be due to two basically different causes, (1) a rotational motion of molecular dipoles with frictional losses, and (2) a translational motion of free electric charges. The former cannot give rise to d.c. conductivity, σ_0, while the latter can. Debye [16] has applied the concept of rotating dipoles to explain the dispersion of a.c. properties with frequency. An alternative approach to explain the a.c. conductivity is by considering the motion of free charges in a dielectric. The charges are considered to move by discontinuous hopping jumps between well-defined localized sites, spending most of the time at rest on these sites. This hopping conductivity should be clearly distinguished from free-band conduction and its frequency dependence can be summarized with reference to Fig. 11 at sufficiently low frequencies and down to d.c. there is a constant level, σ_0, which may or may not be accessible experimentally within the limitions of low-field conditions in which conductivity may really be defined. There follows a region in which the conductivity is a monotonically increasing function of frequency.

$$\sigma \propto \omega^s \tag{7}$$

where s takes typical values in the range $0.5 < s < 1$. This region is relatively well documented experimentally for a wide range of materials in which conduction occurs by hopping [17–19], as distinct from free band conduction. The estimated values for s at a frequency of 2×10^4 Hz are shown in Figs 9a, b and c for different compositions. Pollak and Geballe [20] have studied the a.c. properties of compensated silicon at very low tempertures – a classic example of a hopping system. Since then many more disordered and amorphous or glassy materials have been found to exhibit the same type of behaviour. It is noted that the exponent s in the power-law Equation 7 is temperature dependent at low frequencies and varies between zero, i.e. d.c. conduction at high temperatures, through 0.5 at intermediate temperatures to 1 at low temperatures, and s varies between 1 and 2 at high frequencies. The second significant point is that there is no well-defined activation energy in these results (Figs 10a, b and c), rather as for d.c. conduction through traps [21].

Figs 12a and b show the variations of capacitance with temperature and frequency for two samples of different compositions. The total measured capacitance, $C_{\text{tot}}(\omega)$, can be decomposed into two components, a dispersive term, $C(\omega)$, and a non-dispersive term, C_∞,

$$C_{\text{tot}}(\omega) = C(\omega) + C_\infty \tag{8}$$

These two components arise from different processes, C_∞ being due to high-frequency atomic and dipolar

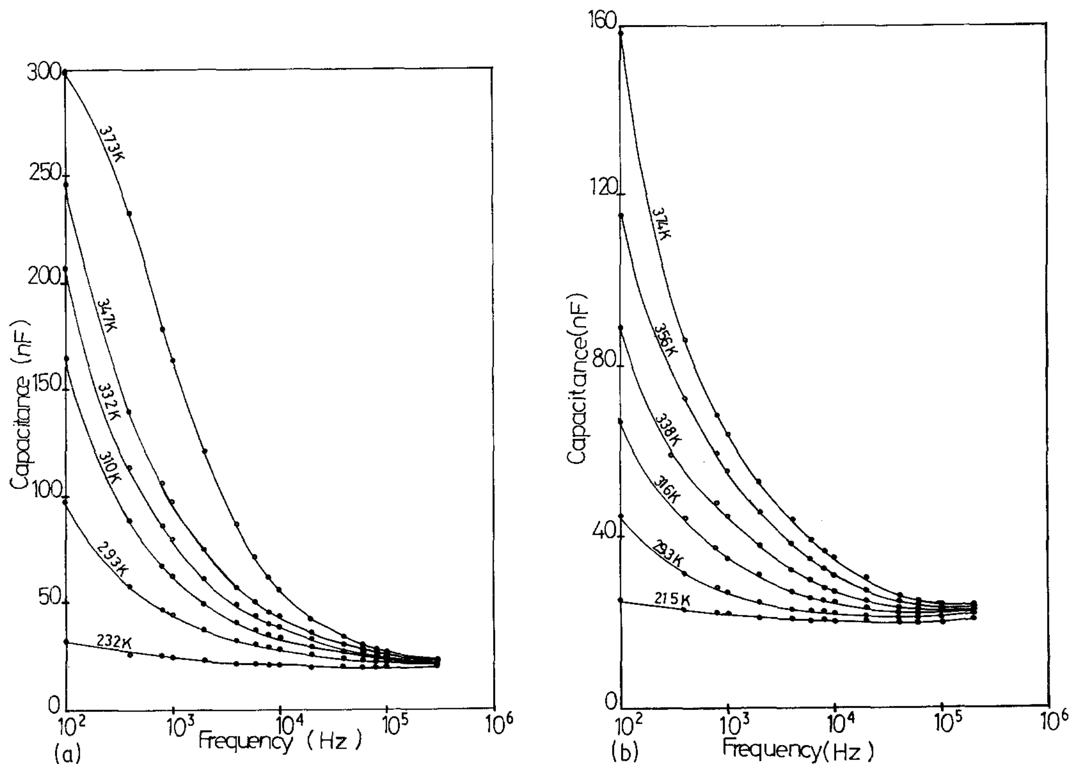

Figure 12 Variation of capacitance with frequency at different temperatures. (a) 60 mol % CeO_2/40 mol % GeO_2, (b) 40 mol % CeO_2/60 mol % GeO_2.

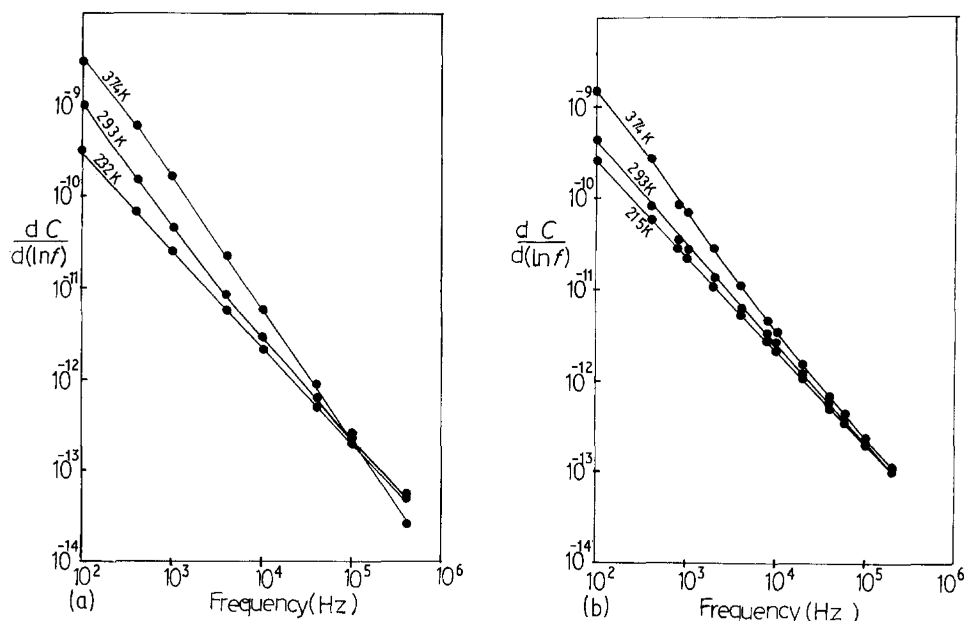

Figure 13 Variation of $dC/d(\ln f)$ with frequency for the samples in Fig. 12.

vibrational transitions, whereas $C(\omega)$ is determined by the loss mechanisms. Different methods used for eliminating the non-dispersive component exist, e.g. measurement at high frequencies (where $C_\infty(\omega) \rightarrow C_\infty$), adjustment of C_∞ until the resulting $C(\omega)$ obeys a power-law dependence, or numerical differentiation of the capacitance data, whereupon the constant terms involving C_∞ drop out. Thus, if the dispersive part of the capacitance obeys the power law

$$C(\omega) \sim \omega^{s'-1} \quad (9)$$

(where s' is not equal to s, the frequency exponent for the real part of the conductivity), a plot of log (d C/d ln f) against log f should yield a straight line of slope $s' - 1$ as shown in Figs 13a and b. It is noted that the slope $s' - 1$ decreases as the temperature decreases (i.e. s' and s behave in a qualitatively similar manner).

References

1. Z. T. AL-DHHAN and C. A. HOGARTH, *Int. J. Electron.* **63** (1987) 707.
2. I. M. KHAN, C. A. HOGARTH and M. N. KHAN, *ibid.* **46** (1979) 215.
3. M. N. KHAN, M. I. KHAN and C. A. HOGARTH, *Phy. Rev. B* **22** (1980) 6155.
4. C. A. HOGARTH and A. S. M. S. RAHMAN, *Thin Solid Films* **87** (1982) L3.
5. F. A. S. AL-RAMADHAN, C. A. HOGARTH and K. I. ARSHAK, *Int. J. Electron.* **57** (1984) 227.
6. C. A. HOGARTH and L. A. WRIGHT, Proceedings International Conference on Physics of Semiconductors, Moscow (Nauka, Leningrad, 1968) p. 1274.
7. W. SCHOTTKY, *Physik. Z.* **15** (1914) 872.
8. J. FRENKEL, *Phys. Rev.* **54** (1938) 647.
9. N. MOTT, "Conduction in Non-crystalline Materials" (Clarendon, Oxford, 1987).
10. R. M. ROSE, L. A. SHEPARD and J. WULFF, "The Structure and Properties of Materials", Vol. IV, Electronic Properties (Wiley, New York, London, Sydney, 1968).
11. G. DEARNALEY, D. V. MORGAN and A. M. STONEHAM, *J. Non-Cryst. Solids* **4** (1970) 593.
12. G. DEARNALEY, *Thin Solid Films* **3** (1967) 161.
13. J. G. SIMMONS and R. R. VERDERBER, *Proc. R. Soc. Lon. Ser. A* **301** (1967) 77.
14. J. E. RALPH and J. M. WOODCOCK, *J. Non-Cryst. Solids* **7** (1972) 236.
15. P. DEBYE, "Polar Molecules" (Chemical Catalog Co., New York, 1929).
16. V. DANIEL, "Dielectric Relaxation" (Academic, New York, 1967).
17. H. FRITZSCHE and M. CUEVAS, *Phys. Rev.* **119** (1960) 1238.
18. A. MILLER and E. EBRAHAM, *Phys. Rev.* **120** (1960) 745.
19. N. F. MOTT and W. D. TWOSE, *Adv. Phys.* **10** (1961) 107.
20. M. POLLAK and T. H. GEBALLE, *Phys. Rev.* **122** (1961) 1742.
21. R. M. HILL, *Phil. Mag.* **24** (1971) 1307.

Received 29 June
and accepted 22 September 1987